Front. Phys. 13(4), 135202 (2018)
https://doi.org/10.1007/s11467-018-0788-9

RESEARCH ARTICLE

Photon and positron generation by ultrahigh intensity laser interaction with electron beams

Muhammad Ali Bake[†], Aimierding Aimidula[‡], Arkin Zakir, Nuriman Abdukerim, Abduleziz Ablat

School of Physics Science and Technology, Xinjiang University, Urumqi 830046, China
Corresponding authors. E-mail: [†]aili@mail.bnu.edu.cn, [‡]amir@mail.bnu.edu.cn
Received November 6, 2017; accepted April 10, 2018

This study investigates the generation of high energy photons and positrons using focused ultrahigh intensity femtosecond laser pulses on a relativistic electron beam with a set of two-dimensional particle-in-cell simulations. We consider circularly and linearly polarized, single and spatially separated double laser pulses. We model both 500 MeV and 1 GeV electron beams. Higher positron production is obtained using circularly polarized laser pulses. Using double pulses, the focusing effect of the ponderomotive force confines the electrons to a small volume, generating additional energetic photons and positrons. The positron spectral distributions are effectively modified by these variations. When the electron beam energy is doubled, the number of positrons increased, while the cutoff energy remained nearly constant.

Keywords laser-electron beam interaction, photon and positron generation, QED effect

PACS numbers 52.38.Kd, 52.38.Hb, 52.65.Rr

1 Introduction

One of the most interesting applications of ultra-intense laser pulses is the acceleration of charged particles to high energies. This has been intensively investigated recently for its potential in table-top accelerators [1–3] and other uses in many fields [3–5].

With the advancement of laser technologies and experimental capabilities, peak intensities have increased while pulse durations have shortened [6]. Petawatt (PW) scale laser systems are currently being conceived. The generation of 10–100 PW is envisioned in the Extreme Light Infrastructure beamlines project underway in central Europe [7]. By tightly focusing such a laser pulse, intensities of up to 10^{24} W/cm^2 are achievable, whereupon many phenomena in quantum electrodynamics (QED) can be attained in the laboratory, such as high energy gamma ray emission and electron-positron pair generation [8, 9]. Potential uses of gamma ray and positron beams include fundamental nuclear and particle physics research [10] and laboratory astrophysics and plasma physics analogs for interpreting celestial events [11, 12], as well as others. These high-energy beams will not only provide deep insights into fundamental physics, but will also enable novel experimental applications.

Considerable theoretical and numerical studies into different physical mechanisms taking place in QED phenomena have been undertaken [13–22]. Recently, several reports have predicted that ultra-intense laser fields could induce QED cascades, which would be abundant sources of photons and electron-positron pairs [17, 19, 21–23]. Various mechanisms have been proposed to explain high energy photon emission and electron-positron pair production processes [24–29]. The three most extensively investigated of these are the trident process [26–28], the Bethe–Heitler (BH) process [24], and the Breit–Wheeler (BW) process [25]. In the Trident process, positrons are produced directly by energetic electrons interacting with the Coulomb field of the atomic nucleus: $(Z + e^- \rightarrow Z + 2e^- + e^+)$ [27, 28]. This type of pair creation can result from relatively moderate laser intensities $I \sim 10^{22}$ W/cm^2, but the positron yields are too low for practical applications. In the BH process, electron-positron pairs are generated by nuclei interacting with gamma photons radiated from decelerated electrons in the target via Bremsstrahlung radiation: $(\gamma + Z \rightarrow Z + e^- + e^+ + \gamma')$ [24]. This is important only for high-Z nuclei and moderate laser intensities. In the BW process, plasma electrons are first accelerated by the laser field such that they radiate a significant fraction of their energy as gamma-ray photons by strongly non-

linear inverse Compton scattering ($\gamma_{laser}+e^- \rightarrow \gamma+e^+$). Then, the emitted gamma-ray photons generate electron-positron pairs in the laser field by the multiphoton Breit-Wheeler process ($\gamma + n\gamma_{laser} \rightarrow e^- + e^+$) [25], which generates further photons and electron-positron pairs, resulting in a cascade of pair production [18]. This process dominates in ultrahigh intensity laser fields. Quantum effects for electron dynamics in strong laser fields are governed by the invariant parameter $\chi = |F_{\mu\nu}P^{\nu}|/mE_s$, where $F_{\mu\nu}$ is the electromagnetic field tensor and $P^{\nu} = \gamma m(c, \boldsymbol{v})$ is the four-momentum of the electron (Planck units $\hbar = c = 1$ are used throughout). Physically, χ is the ratio of the electric field in the electron rest frame to the critical Schwinger field $E_s = m^2/e$, and the BW process is considerable only if $\chi > 1$. The laser intensity corresponding to the Schwinger field is $\sim 2.3 \times 10^{29}$ W/cm^2 which cannot be reached with realistic lasers [41, 42]. However, a relativistic electron counter propagating with the laser field has $\chi \approx 1$ due to the Lorentz boost, where quantum emission effects become important.

Experimentally, pair production by laser-electron interaction was demonstrated at the Stanford Linear Accelerator Center in 1997 [30]. In this experiment, a 46.6 GeV electron beam collided with a counter-propagating laser beam, generating electron-positron pairs [31]. The physical process occurs via two steps. First, high-energy photons are emitted from nonlinear Compton scattering of laser photons with relativistic electrons. Second, the electron-positron pairs are created by these high-energy photons interacting with multiple laser photons through the BW process. If a QED cascade can be triggered in the laboratory, dense beams of positrons will be produced, enabling several new fields, including antimatter science [32], pair plasma physics [15–21], and the reproduction of astrophysical phenomena [12].

In this paper, we present simulations of head-on collisions between ultrahigh intensity laser pulses and relativistic electron beams, yielding high-energy photons and positrons. We modeled both linearly polarized (LP) and circularly polarized (CP) laser beams, as well as two different electron beam energies. In addition, we carried out calculations using a time-coincident but spatially separated double beam shaped laser profile. We found that positron creation was significantly enhanced using CP radiation relative to LP. Photon and positron production using double CP lasers exceeded that of a single CP laser. When the electron beam energy is doubled, the number of photons and positrons increase while the cut-off energy of both remain nearly constant. Thus, a QED cascade may be more easily triggered by double CP laser pulses and higher electron beam energy.

We use the quantum electrodynamics particle-in-cell (QED-PIC) code EPOCH [34] to simulate photon emission and electron-positron pair production in the laser-electron beam interaction process. Section 2 will introduce the physical model and the PIC simulation parameters. In Section 3, we study the results for photon emission and positron production by different laser pulses and electron beams, present comparisons between them, and include some discussion. Finally, in Section 4, we provide a summary of our work.

2 Model and simulation parameters

Our physical model is illustrated in Fig. 1. First, we consider the simple geometry of a single laser pulse interacting with the electron beam, as shown in Fig. 1(a). We begin by examining the two laser polarization states. The CP electric field rotates about the x axis and oscillates along the y axis in LP laser pulses. Second, we study multiple laser pulses interacting simultaneously with the electron beam, as shown in Fig. 1(b). In the double pulse configuration, the laser pulses are transversely separated by equal distances from the electron beam propagation axis. Such multiple pulses could be produced by the fiber laser proposed by Mourou *et al.* [35] or through tailoring the wavefront with a deformable mirror [36]. In the 2D simulations, two parallel CP or LP laser pulses are positioned at the right side of the simulation box [36]. They have identical Gaussian temporal profiles and the same spatial widths.

To test our proposed idea, we carried out a set of 2D QED-PIC simulations for the different configurations mentioned above. Photon emission and electron-positron pair creation via the BW process were modeled using the

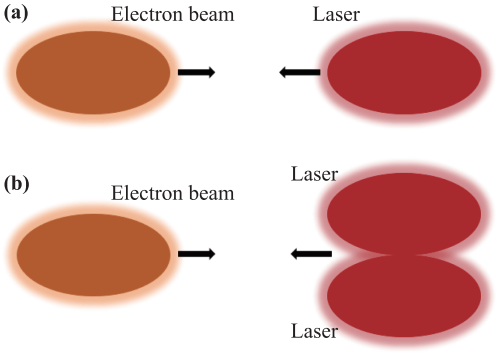

Fig. 1 Structural diagram of our proposed scheme. **(a)** A single laser pulse interacting with a counter-propagating electron beam. **(b)** Multiple laser pulses interacting with a counter-propagating electron beam. The laser pulse enters the simulation box from the right boundary at $t = 0$, and propagates along the negative x direction. The electron beam enters the simulation box from the left boundary at $t = 0$, propagating in the positive x direction. Other model parameters are given in the text.

Monte Carlo method. In our simulations, the laser pulses enter the simulation box from the right boundary at $t = 0$, propagate along the negative x direction, and collide head-on with the counter-propagating electron beam. The laser has a wavelength $\lambda = 1$ μm and peak intensity $I = 3 \times 10^{24}$ W/cm^2, which corresponds to a normalized laser amplitude of $a_0 = eA/(m_e c^2) = 1480/\sqrt{2}$ for CP and $a_0 = 1480$ for LP, where e is the electron charge, A is the vector potential, m_e is the electron rest mass, and c is the speed of light in vacuum. The laser has a Gaussian intensity profile $a = a_0 \exp[-(y/y_0)^2 - (t/T_L)^2]$ with a focal spot of $y_0 = 3$ μm and duration of $T_L = 30$ fs. In simulations with two laser pulses, the center-to-center separation between two laser pulses is 6 μm, which matches the electron beam diameter. In this way, we can control the electrons between the two laser pulses. If the separation width were made shorter or longer than the electron-beam diameter, electrons would flow away from the upper and lower edge of the beam or between the two laser pulses. Centered on the y-axis at $x = 10\lambda$ on the left side of the simulation box is an electron cloud with a FWHM $w_0 = 3$ μm, which is represented by 1×10^7 total macroscopic particles. The electron-beam has a Gaussian density profile and the duration is 30 fs. The longitudinal and transverse initial temperatures of the electrons are 1 MeV and 0.01 MeV. In a moving reference frame, the electron cloud can be considered as a bunch of electrons moving left to right in the simulation box. The electron-beam energy is set at either 500 MeV or 1 GeV. In a table-top environment, electron beams with energies of 500 MeV to 4 GeV can be obtained by laser wakefield acceleration [37–39], which could then be collided with laser pulses to create photons and electron-positron pairs [40]. The size of simulation box is 50 μm (x) × 30 μm (y), gridded at 2000 × 900 cells. The boundary conditions are periodic in the transverse direction and simple-outflow longitudinally.

3 Simulation results and discussion

We begin with a simulation of a single laser pulse interacting with a 500 MeV electron beam. As electron motion is critical to generating high energy photons and positrons, significant differences result from CP versus LP laser pulses. Figure 2 shows the density distributions of electrons, photons, and positrons for both polarizations at $t = 96$ fs. The results reveal that dynamically, the electrons decelerate first, reverse direction, and then accelerate parallel to the laser propagation direction. The laser field ponderomotive force develops the cone shaped electron density distributions for both laser polarizations, as shown in Figs. 2(a) and (b). A greater electron concentration develops with the CP pulse. Figures 2(c) and (d) show the density distributions of the

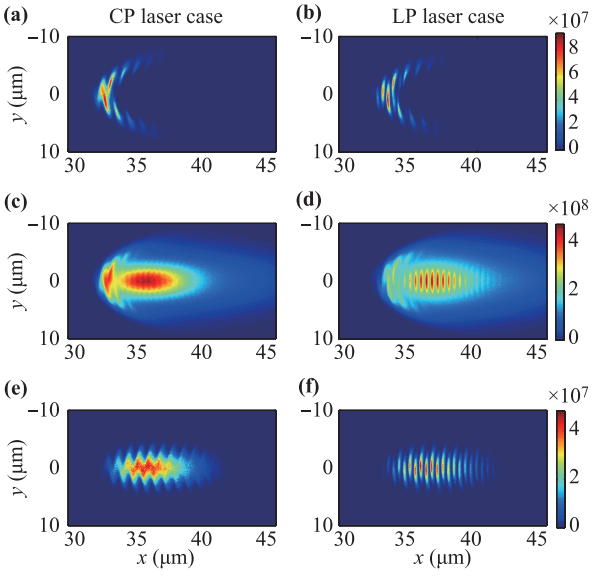

Fig. 2 Electron, photon and positron density distributions at $t = 96$ fs. The left column **(a)**, **(c)**, and **(e)** are for CP laser pulses, and the right column **(b)**, **(d)**, and **(f)** are for LP laser pulses. The electron beam initial energy is 500 MeV, and other parameters of the laser and electron beam are as defined in text. x is the electron beam propagation and laser counter-propagation direction, and y is the transverse direction.

high-energy photons. For a CP laser pulse, the photons are mostly distributed in the front and inside of the cone structure. However, for LP, the photons are mostly distributed inside the cone with sharp spatial modulation. Figures 2(e) and (f) show the positron density distributions. For a CP pulse, the positrons show a zigzag profile, where the peak density for any given longitudinal position x oscillates slightly above and below $y = 0$. In contrast, for an LP pulse, the positrons show a strip-like profile. Notably, all three CP distributions in Fig. 2 show zigzag profiles, while all three LP profiles feature strip-like modulation. This results from rotation of the laser electric field around the x axis in CP versus oscillation along the y axis in LP. Consequently, electrons exposed to CP undergo helical motion, while with LP they undergo linear oscillations. Since photon emission from relativistic electrons is narrowly confined along the electron motion direction, the photon and positron densities follow the electron distribution profile.

Figure 3 shows the energy spectra of electrons, photons, and positrons for both CP and LP laser pulses at $t = 96$ fs. From Fig. 3(a), no larger differences were observed in the electron cutoff energy between the two polarizations, while the energy spectrum was wider for LP pulses. Figure 3(b) shows the photon spectra for both polarizations. CP pulses result in a higher energy tail, with a cutoff at 5 GeV versus only 3 GeV for LP pulses. From the positron energy spectra in Fig. 3(c), both laser

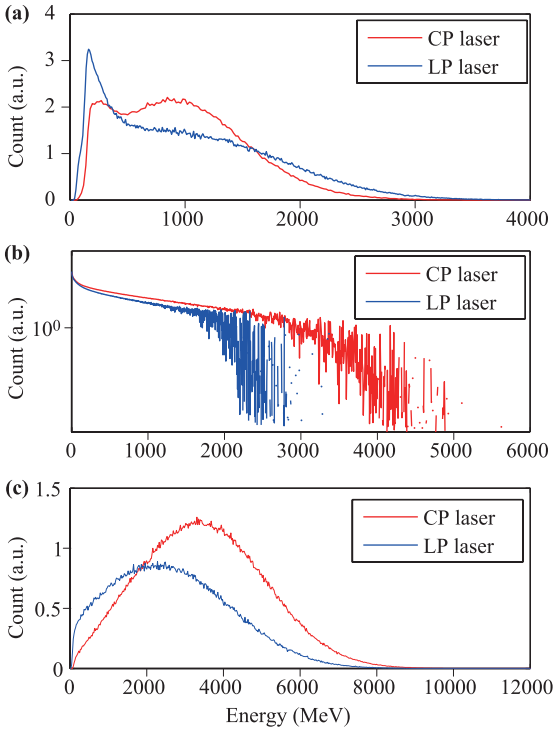

Fig. 3 Energy spectra for both the CP laser (red) and LP laser (blue) pulses at $t = 96$ fs. **(a)** is the electron energy spectrum, **(b)** the photon energy spectrum, and **(c)** the positron energy spectrum. The electron beam initial energy is 500 MeV. Other parameters are as defined in Fig. 2.

polarizations show a cutoff energy around 8 GeV. However, the positron peak energy of 4 GeV for CP is shifted well above the 2 GeV peak for LP, and the number of positrons is also higher for CP.

The results shown in Figs. 2 and 3 indicate that more high energy photons and positrons can be generated using a CP laser pulse compared to using an LP laser pulse. Choosing the proper laser pulse polarization is crucial in the laser electron beam collision QED process, with CP pulses being particularly advantageous. Next, we investigate the physical processes of double laser pulses interacting with a 500 MeV electron beam. Following our single beam outcome, we used CP laser pulses, and single CP results will be compared with double CP pulses. Figures 4(a) and (b) display the electron density distribution at $t = 96$ fs. The ponderomotive forces between the pulse centers in the double pulse configuration tightly focus electrons to a cone pattern from a single pulse. High-energy photon and positron density distributions are shown in Figs. 4(d) and (f). Most of the photons are generated in the compact region where the electrons are focused. Comparing Figs. 4(e) and (f) one sees similar zigzag positron profiles. However, in the double pulse calculation, the positron areal footprint is larger than that for the single pulse, meaning more positrons are created in the double pulse interaction, which can also be seen in Fig. 5.

Figure 6 displays the electron, photon, and positron energy spectra for both single and double pulses at $t = 96$ fs. The electron energy spectra in Fig. 6(a) shows a narrower double pulse FWHM, consistent with the ponderomotive focusing shown in Fig. 4(b). The photon energy spectrum in Fig. 6(b) shows a broader energy tail than for a single pulse. The positron spectra are shown in Fig. 6(c). As surmised from the spatial extent result in Figs. 4(e) and (f), positron production from a double pulse is higher than from a single pulse. The peak energy is slightly larger, while the cut-off energies are nearly identical.

Finally, we investigate how the initial energy of the electron beam affects positron production. We carried out PIC simulations for both single and double CP pulses incident on a 1 GeV electron beam. Figure 7 shows a comparison between the electron, photon, and positron spectra from single and double pulses, at $t = 96$ fs. The width of the double pulse electron spectrum is narrower than for the single pulse, just as was observed for the 500 MeV electron beam. Similarly, the double pulse photon spectrum shows a broad high-energy tail that exceeds the single pulse result. Likewise, more positrons are produced at 1 GeV with the double pulse, which is consistent with the result from the 500 MeV electron beam. The trends observed for all three metrics in the single versus double CP pulse comparison at 1 GeV are very similar to the trends observed at 500 MeV.

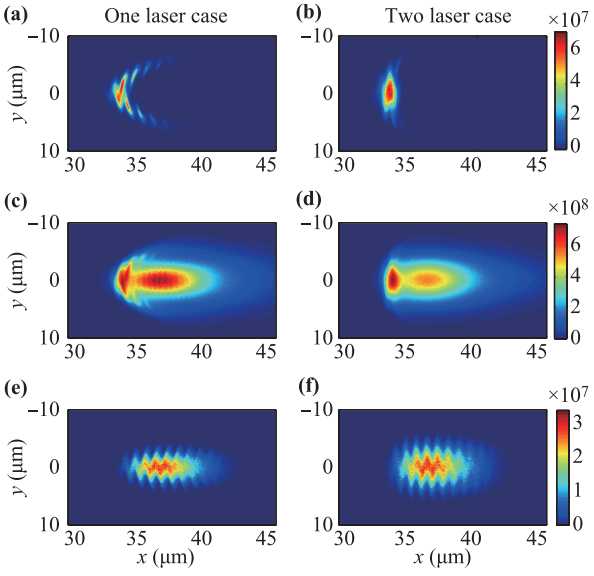

Fig. 4 Electron, photon and positron density distributions at $t = 96$ fs for single (left column) and double (right column) CP laser pulses. The electron beam initial energy is 500 MeV. Other parameters are as defined in Fig. 2.

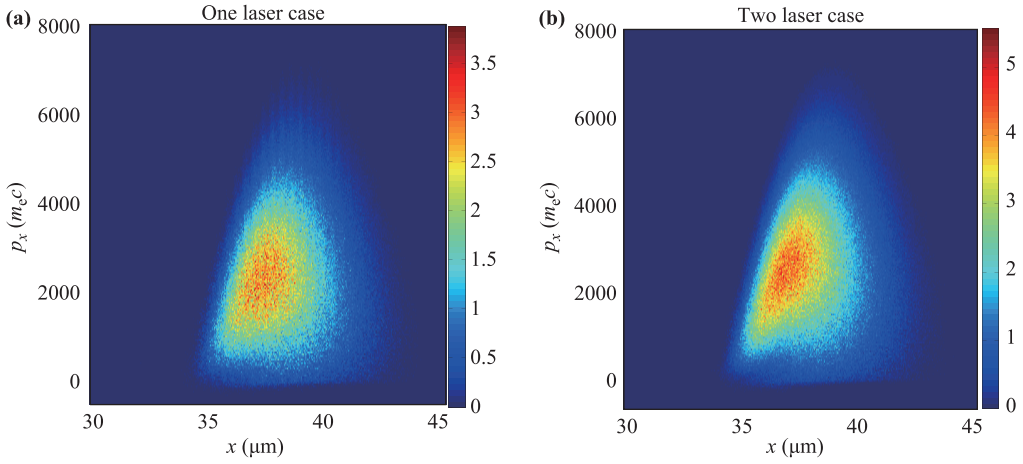

Fig. 5 Phase space distribution of positrons $(x - p_x)$ at $t = 96$ fs. **(a)** for single laser pulses and **(b)** for double laser pulses. The electron beam initial energy is 500 MeV. Other parameters are as defined in Fig. 2.

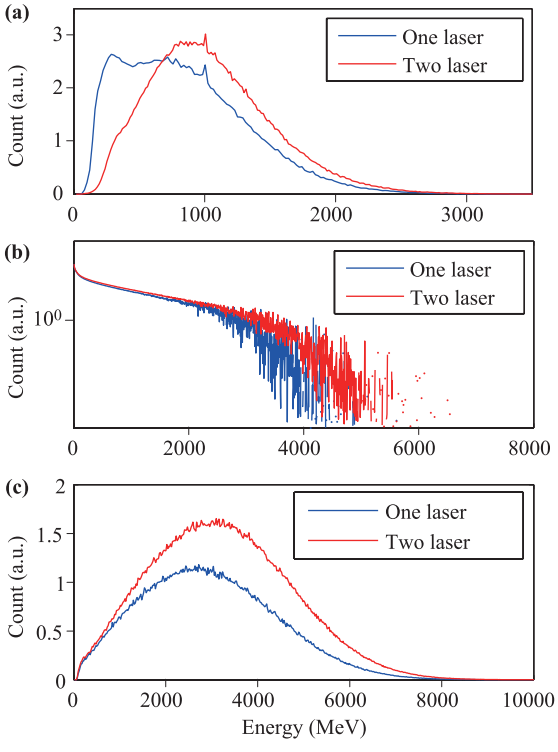

Fig. 6 Energy spectra for single (blue) and double (red) CP laser pulses at $t = 96$ fs. **(a)** is the electron energy spectrum, **(b)** the photon energy spectrum, and **(c)** the positron energy spectrum. The electron beam initial energy is 500 MeV. Other parameters are as defined in Fig. 2.

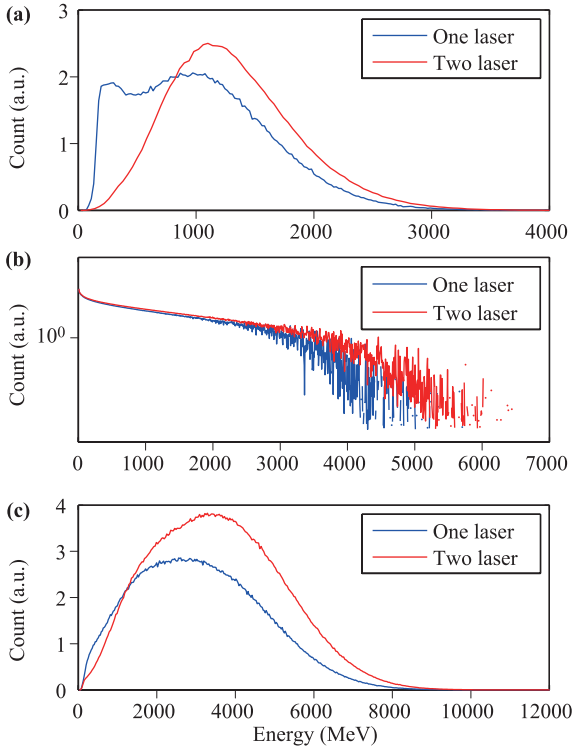

Fig. 7 Energy spectra with a 1 GeV electron beam for both double CP (red) and single CP (blue) pulses at $t = 96$ fs. **(a)** is the electron energy spectrum, **(b)** is the photon energy spectrum, and **(c)** is the positron energy spectrum. Other parameters are as defined in Fig. 2.

In Fig. 8, CP double pulse results at 1 GeV electron beam energy are compared directly to those at 500 MeV. The electron and photon spectra, as shown in Figs. 8(a) and (b), show no substantial differences. However, the number of positrons significantly increased at 1 GeV. The positron cutoff energy is largely unchanged.

From the results shown in Figs. 4–8, the CP double pulse configuration is recommended to maximize photon and positron production by laser electron beam interaction. The high-energy photons and positrons produced

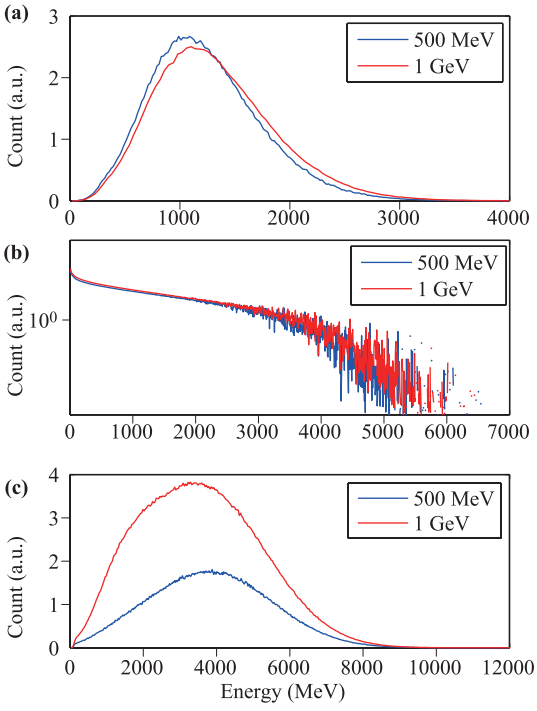

Fig. 8 Energy spectra comparing the 500 MeV (blue) and 1 GeV (red) electron beam energies at $t = 96$ fs. **(a)** is the electron energy spectrum, **(b)** is the photon energy spectrum, and **(c)** is the positron energy spectrum. Other parameters are as defined in Fig. 2.

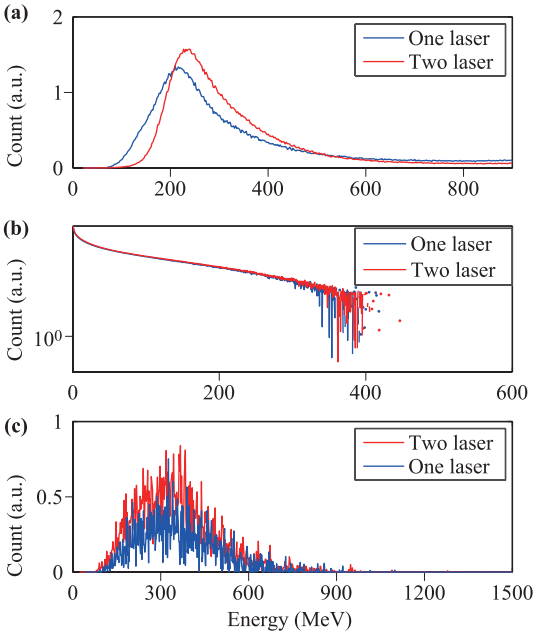

Fig. 9 Energy spectra for single (blue) and double (red) CP laser pulses with peak intensity $I = 1.3 \times 10^{23}$ W/cm^2 at $t = 96$ fs. **(a)** is the electron energy spectrum, **(b)** the photon energy spectrum, and **(c)** the positron energy spectrum. The electron beam initial energy is 500 MeV. Other parameters are as defined in Fig. 2.

may have diverse applications.

The laser intensity used in simulations above is too large and too far away from the present laser technology. Therefore, we consider more reasonable laser intensity done some simulations. We carried out a set of 2D QED-PIC simulations for the PC laser pulses with peak intensity $I = 1.3 \times 10^{23}$ W/cm^2, which corresponds to a normalized laser amplitude of $a_0 = 316$. The remaining parameters were left unchanged. Figure 9 shows the energy spectra of electrons, photons, and positrons at $t = 96$ fs. Figure 9(a) shows that the peak energies and corresponding number of electrons are slightly higher for the double pulse, while the cut-off energies are nearly identical. Figure 9(b) shows the photon spectra for both single and double laser pulses. There were no major differences in the photon energy spectra between the two cases. From the positron energy spectra in Fig. 9(c), both laser cases show almost same peak and cutoff energy around 0.9 GeV. However, the number of positrons is slightly higher for the double laser. The results shown in Figs. 6 and 9 that more high energy photons and positrons can be generated using a high intensity laser pulse, which means that the laser intensity is crucial in the laser electron beam collision QED process, with higher intensity pulses being particularly advantageous.

It should be noted that the maximum positron energy is higher than the initial seed photons in all cases, as shown in Figs. 3, 6, 7, 8, and 9. This can generally be attributed to the fact that the positrons, which are produced by the initial gamma-ray photons, will experience direct laser ponderomotive acceleration for some time, and they gain some additional energy from the laser. Therefore, the maximum energy of the positrons is higher than the initial energy of the seed photons.

4 Summary

In this paper, we studied the interactions between a relativistic electron beam and ultrahigh intensity femtosecond laser pulses in order to provide a reference for future QED experiments. The simulations are conducted with the help of the 2D QED-PIC code EPOCH. The effects of single and double laser pulses were investigated, and electron beams with different initial energies were used to generate high-energy photons and positrons.

First, we investigated the effect of laser polarization on photon emission and electron-positron pair production efficiencies. The simulation results show that a CP laser pulse produces photon and positron with higher probability than an equivalent intensity LP laser pulse.

Second, by comparatively evaluating the particle density distributions and energy spectra of the photons and positrons, we found that double pulses create a larger number of particles that extend to higher energies than the single pulses. When the electron beam energy in an optimized double CP laser pulse configuration was doubled, we found a significant increase in positron production with no change in the cutoff energy. Finally, we considered a more reasonable laser intensity available in practical applications, and we found that the laser plays a key role in the electron beam collision QED process.

We believe that our results help deepen the understanding of QED processes under extreme conditions, while also enabling useful applications. We hope to initiate a possible means of obtaining a high quality photon and positron source, which is important in many applications which is important in many applications such as pair plasma physics, fundamental nuclear and particle physics research, and laboratory astrophysics.

Acknowledgements This work was financially supported by the National Natural Science Foundation of China (NSFC) (Grant Nos. 11664039 and 11575150), and the Doctoral Fund of Xinjiang University (Grant Nos. BS150216 and BS150217). A. Ablat was supported by NSFC (Grant Nos. 61464010 and 61604126). The authors are particularly grateful to CFSA at the University of Warwick for allowing us to use the EPOCH.

References and notes

1. E. Esarey, C. B. Schroeder, and W. P. Leemans, Physics of laser-driven plasma-based electron accelerators, *Rev. Mod. Phys.* 81(3), 1229 (2009)
2. S. M. Hooker, Developments in laser-driven plasma accelerators, *Nat. Photon.* 7(10), 775 (2013)
3. A. Macchi, M. Borghesi, and M. Passoni, Ion acceleration by superintense laser-plasma interaction, *Rev. Mod. Phys.* 85(2), 751 (2013)
4. H. Daido, M. Nishiuchi, and A. S. Pirozhkov, Review of laser-driven ion sources and their applications, *Rep. Prog. Phys.* 75(5), 056401 (2012)
5. B. A. Remington, R. P. Drake, and D. D. Ryutov, Experimental astrophysics with high power lasers and *Z* pinches, *Rev. Mod. Phys.* 78(3), 755 (2006)
6. G. A. Mourou, T. Tajima, and S. V. Bulanov, Optics in the relativistic regime, *Rev. Mod. Phys.* 78(2), 309 (2006)
7. E. L. I. Beamlines, www.eli-beams.eu
8. F. Ehlotzky, K. Krajewska, and J. Z. Kaminski, Fundamental processes of quantum electrodynamics in laser fields of relativistic power, *Rep. Prog. Phys.* 72(4), 046401 (2009)
9. A. Di Piazza, C. Müller, K. Z. Hatsagortsyan, and C. H. Keitel, Extremely high-intensity laser interactions with fundamental quantum systems, *Rev. Mod. Phys.* 84(3), 1177 (2012)
10. S. Gales, D. L. Balabanski, F. Negoita, O. Tesileanu, C. A. Ur, D. Ursescu, and N. V. Zamfir, New frontiers in nuclear physics with high-power lasers and brilliant monochromatic gamma beams, *Phys. Scr.* 91(9), 093004 (2016)
11. E. Liang, Gamma-ray and pair creation using ultra-intense lasers and astrophysical applications, *High Energy Density Phys.* 9(3), 425 (2013)
12. P. Chen and G. Mourou, Accelerating plasma mirrors to investigate the black hole information loss paradox, *Phys. Rev. Lett.* 118(4), 045001 (2017)
13. A. A. Gonoskov, I. Gonoskov, C. Harvey, A. Ilderton, A. Kim, M. Marklund, G. Mourou, and A. Sergeev, Probing nonperturbative QED with optimally focused laser pulses, *Phys. Rev. Lett.* 111(6), 060404 (2013)
14. M. Vranic, T. Grismayer, R. A. Fonseca, and L. O. Silva, Quantum radiation reaction in head-on laser-electron beam interaction, *New J. Phys.* 18(7), 073035 (2016)
15. T. G. Blackburn, C. P. Ridgers, J. G. Kirk, and A. R. Bell, Quantum radiation reaction in laser–electron-beam collisions, *Phys. Rev. Lett.* 112(1), 015001 (2014)
16. I. V. Sokolov, N. M. Naumova, J. A. Nees, and G. A. Mourou, Pair creation in QED-strong pulsed laser fields interacting with electron beams, *Phys. Rev. Lett.* 105(19), 195005 (2010)
17. A. R. Bell and J. G. Kirk, Possibility of prolific pair production with high-power lasers, *Phys. Rev. Lett.* 101(20), 200403 (2008)
18. C. P. Ridgers, C. S. Brady, R. Duclous, J. G. Kirk, K. Bennett, T. D. Arber, and A. R. Bell, Dense electron-positron plasmas and bursts of gamma-rays from laser-generated quantum electrodynamic plasmas, *Phys. Plasmas* 20(5), 056701 (2013)
19. C. P. Ridgers, C. S. Brady, R. Duclous, J. G. Kirk, K. Bennett, T. D. Arber, A. P. L. Robinson, and A. R. Bell, Dense electron-positron plasmas and ultraintense g rays from laser-irradiated solids, *Phys. Rev. Lett.* 108(16), 165006 (2012)
20. J. R. Danielson, D. H. E. Dubin, R. G. Greaves, and C. M. Surko, Plasma and trap-based techniques for science with positrons, *Rev. Mod. Phys.* 87(1), 247 (2015)
21. S. S. Bulanov, T. Zh. Esirkepov, A. G. R. Thomas, J. K. Koga, and S. V. Bulanov, Schwinger limit attainability with extreme power lasers, *Phys. Rev. Lett.* 105(22), 220407 (2010)
22. M. Jirka, O. Klimo, S. V. Bulanov, T. Zh. Esirkepov, E. Gelfer, S. S. Bulanov, S. Weber, and G. Korn, Electron dynamics and g and e^-e^+ production by colliding laser pulses, *Phys. Rev. E* 93(2), 023207 (2016)
23. T. Grismayer, M. Vranic, J. L. Martins, R. A. Fonseca, and L. O. Silva, Seeded QED cascades in counterpropagating laser pulses, *Phys. Rev. E* 95(2), 023210 (2017)

24. S. Augustin and C. Müller, Interference effects in Bethe-Heitler pair creation in a bichromatic laser field, *Phys. Rev. A* 88(2), 022109 (2013)
25. K. Krajewska and J. Z. Kami'nski, Breit-Wheeler process in intense short laser pulses, *Phys. Rev. A* 86(5), 052104 (2012)
26. B. F. Shen and J. Meyer-ter-Vehn, Pair and g -photon production from a thin foil confined by two laser pulses, *Phys. Rev. E* 65(1), 016405 (2001)
27. H. Y. Hu, C. Müller, and C. H. Keitel, Complete QED theory of multiphoton trident pair production in strong laser fields, *Phys. Rev. Lett.* 105(8), 080401 (2010)
28. A. Ilderton, Trident pair production in strong laser pulses, *Phys. Rev. Lett.* 106(2), 020404 (2011)
29. S. Tang, M. A. Bake, H. Y. Wang, and B. S. Xie, QED cascade induced by a high-energy γ photon in a strong laser field, *Phys. Rev. A* 89, 022105 (2014)
30. D. L. Burke, R. C. Field, G. Horton-Smith, J. E. Spencer, D. Walz, S. C. Berridge, W. M. Bugg, K. Shmakov, A. W. Weidemann, C. Bula, K. T. McDonald, E. J. Prebys, C. Bamber, S. J. Boege, T. Koffas, T. Kotseroglou, A. C. Melissinos, D. D. Meyerhofer, D. A. Reis, and W. Ragg, Positron production in multiphoton light-by-light scattering, *Phys. Rev. Lett.* 79(9), 1626 (1997)
31. C. Bamber, S. J. Boege, T. Koffas, T. Kotseroglou, A. C. Melissinos, D. D. Meyerhofer, D. A. Reis, W. Ragg, C. Bula, K. T. McDonald, E. J. Prebys, D. L. Burke, R. C. Field, G. Horton-Smith, J. E. Spencer, D. Walz, S. C. Berridge, W. M. Bugg, K. Shmakov, and A. W. Weidemann, Studies of nonlinear QED in collisions of 46.6 GeV electrons with intense laser pulses, *Phys. Rev. D* 60(9), 092004 (1999)
32. M. Amoretti, C. Amsler, G. Bonomi, A. Bouchta, P. Bowe, et al., Production and detection of cold antihydrogen atoms, *Nature* 419(6906), 456 (2002)
33. A. N. Timokhin, Time-dependent pair cascades in magnetospheres of neutron stars (I): Dynamics of the polar cap cascade with no particle supply from the neutron star surface, *Mon. Not. R. Astron. Soc.* 408(4), 2092 (2010)
34. T. D. Arber, K. Bennett, C. S. Brady, A. Lawrence-Douglas, M. G. Ramsay, N. J. Sircombe, P. Gillies, R. G. Evans, H. Schmitz, A. R. Bell, and C. P. Ridgers, Contemporary particle-in-cell approach to laser-plasma modelling, *Plasma Phys. Contr. Fusion* 57(11), 113001 (2015)
35. G. Mourou, B. Brocklesby, T. Tajima, and J. Limpert, The future is fibre accelerators, *Nat. Photon.* 7(4), 258 (2013)
36. M. L. Zhou, B. Liu, R. H. Hu, Y. R. Shou, C. Lin, H. Y. Lu, Y. R. Lu, Y. Q. Gu, W. J. Ma, and X. Q. Yan, Stable radiation pressure acceleration of ions by suppressing transverse Rayleigh-Taylor instability with multiple Gaussian pulses, *Phys. Plasmas* 23(8), 083109 (2016)
37. W. P. Leemans, A. J. Gonsalves, H. S. Mao, K. Nakamura, C. Benedetti, C. B. Schroeder, C. Tóth, J. Daniels, D. E. Mittelberger, S. S. Bulanov, J. L. Vay, C. G. R. Geddes, and E. Esarey, Multi-GeV electron beams from capillary-discharge-guided subpetawatt laser pulses in the self-trapping regime, *Phys. Rev. Lett.* 113(24), 245002 (2014)
38. X. M. Wang, R. Zgadzaj, N. Fazel, Z. Y. Li, S. A. Yi, et al., Quasi-monoenergetic laser-plasma acceleration of electrons to 2 GeV, *Nat. Commun.* 4, 1988 (2013)
39. M. Mirzaie, S. Li, M. Zeng, N. A. M. Hafz, M. Chen, G. Y. Li, Q. J. Zhu, H. Liao, T. Sokollik, F. Liu, Y. Y. Ma, L. M. Chen, Z. M. Sheng, and J. Zhang, Demonstration of self-truncated ionization injection for GeV electron beams, *Sci. Rep.* 5(1), 14659 (2015)
40. S. Cipiccia, M. R. Islam, B. Ersfeld, R. P. Shanks, E. Brunetti, et al., Gamma-rays from harmonically resonant betatron oscillations in a plasma wake, *Nat. Phys.* 7(11), 867 (2011)
41. N. Abdukerim, Z. L. Li, and B. S. Xie, Electron-positron pair production in the low-density approximation, *Front. Phys.* 10(4), 101202 (2015)
42. Z. L. Li, D. Lu, and B. S. Xie, Dynamically assisted pair production for scalar QED by two fields, *Front. Phys.* 10(2), 101201 (2015)